Critical Collapse of a Nonlinear Schrödinger Field in Newtonian Gravity

by

David Johnny Shinkaruk

A THESIS SUBMITTED IN PARTIAL FULFILLMENT OF
THE REQUIREMENTS FOR THE DEGREE OF

MASTER OF SCIENCE

in

The Faculty of Graduate Studies

(Physics)

THE UNIVERSITY OF BRITISH COLUMBIA

(Vancouver)

April 20 2010

Abstract

While most of the research on critical collapse has involved the general relativistic gravitational field; There have been demonstrations that, for the case of a perfect fluid, similar phenomena arise when the gravitation is Newtonian. This paper will explore critical collapse of a massive scalar field in spherical symmetry coupled to Newtonian gravity. The mathematical model describing the evolution of our field will be taken as a modified version of the newtonian limit of the Einstein-Klein-Gordon equation, entitled the Nonlinear Schrödinger Poisson System (NSP). The purpose of this paper is to develope a deeper insite into the nature of critical collapse and attempt to characterize the nature of the nonlinearity that leads to critical collapse.

Static calculation of the NSP system were carried out to determine the behavour of our system by varying the exponent (α) in the Poisson equation, having the property of gravitational strength. It was found that $\alpha = 2$ and $\alpha = 3$ carried two distinctly different behavours. Due to smoothness of our system in terms of α, it was found that $\alpha = 8/3$ was the threshold between the two behaviours, denoted α_c. Our system gave us strong evidence that for $\alpha < \alpha_c$ static solutions are stable, indicating that blow-up cannot be induced; While $\alpha > \alpha_c$ produces 1-mode unstable static solutions, allowing for blow-up to occur. Static analysis of the stability of our solutions for various α's produced no information to confirm our conjectures.

Time dependent calculations were then performed with the intent of understanding the end behaviour of the NSP system for all α and amplitudes of the initial gaussian (A). Setting α=2, blow-up could not be induced for any A, finding the system seems to scale with A. Increasing the gravitational strength to $\alpha = 3$, it was found that blow up could be induced, and the critical value for A was found to 16 decimal places. Our critical solution was found to be periodic in time, indicative of Type I critical behaviour. Further, $\alpha = 3$ was found to be 1-mode unstable through pertubation analysis, with a corresponding 1-mode excited state static solutions.

Table of Contents

Appendices

List of Figures

Chapter 1

Introduction

While critical collapse has been studied extensively in general relativity, models involving Newtonian gravity remain largely unexplored. Motivated by calculations showing that critical collapse *can* occur in the Newtonian setting for the case of a perfect fluid, we propose to look for models involving a simpler form of matter—namely a scalar field. We thus will consider the dynamics of generalizations of the Schrodinger-Poisson system, and with a restriction to spherical symmetry. Previous work by Andrew Inwood suggests that although the Schrodinger-Poisson system itself does not produce critical behavior, an increase in the strength of the gravitational coupling to the matter field results in Type I critical phenomena. We will extend these studies and consider additional modifications to the system in attempt to produce simple models that capture the essence of critical collapse.

1.1 Modivations

Part of the motivation for the use of scalar fields in these studies is that they are considerably simpler to handle computationally than more astrophysically realistic matter such as perfect fluids [4]. At the same time, the scalar models seem to capture enough of the strong-field gravitational physics that it is reasonable to expect that they can shed light on the more realistic scenarios. There are two main motivating factors for this project: First, we wish to develop a deeper insight into the nature of critical collapse and the related issue of "blow-up" in evolutionary PDEs. Second, we want to characterize, if possible, the nature of the nonlinearity that leads to critical collapse, by looking for models which exhibit critical behaviour, but which, in some sense, are as simple as possible.

There have been demonstrations that, for the case of a perfect fluid, similar phenomena to critical behaviour arises when the gravitation is Newtonian [9]. We thus wish to see whether critical phenomena can also occur for a scalar field interacting with Newtonian gravity. This question was recently addressed by Andrew Inwood [3] who studied the Newtonian limit of the Einstein-Klein-Gordon equations, which results in a model known as the Schrödinger-Poission (SP) system. Restricting attention to spherical symmetry, Inwood provided strong evidence from numerical calculations that there was no critical behaviour or blow-up in the SP model; However, with the correct modification to the SP system, critical solutions could be generated.

The principal aim of this research is to characterize the nonlinearities that are needed for

critical collapse to occur.

1.2 Critical Collapse

Given a set of evolutionary partial differential equations (PDEs), do solutions exist globally for arbitrarily large data? In the early 1990's Choptuik addressed this question in the context of the gravitational collapse of a massless scalar field in spherical symmetry [1]. Solutions of this model describe two distinct end states (t$\rightarrow \infty$): complete dispersal of the scalar field to large distances on the one hand, and black hole formation with partial scalar field dispersal on the other. Choptuik considered the evolution of families of initial data, characterized by a control parameter, p, which could be tuned to generate solutions that interpolated between the two end states. Specifically, it was found that for each family, there was a critical value $p^\star$, such that for $p < p^\star$, the scalar field completely dispersed, while for $p > p^\star$, a black hole formed. Near $p = p^\star$, the solutions approached a universal solution which was independent of the initial data. The behaviour observed near the threshold black hole formation was dubbed critical behaviour due to its similarity to the critical phenomena familiar from statistical mechanical systems.

1.3 Critical Solutions

The critical solutions known thus far, and the black hole thresholds associated with them, come in two broad classes as seen on Fig. 1.1. Type I behaviour is characterized by static or periodic critical solutions, and by the fact that the black hole mass just above threshold is finite (i.e. so that there is a minimum black hole mass that can be formed from the collapse). Type II behaviour is characterized by continuously or discretely self-similar critical solutions (i.e. the additional symmetry is a continuous or discrete scaling symmetry), and by the fact that the black hole mass just above threshold is infinitesimal [2]. The behaviour seen in Choptuik's original study was Type II, while an example of Type I phenomena is provided by the collapse of spherically symmetric boson stars by Hawley and Choptuik [8], which again used a scalar field as a matter source.

Last years results showed as the tuning parameter approached the critical value, the Ψ field became periodic in time from a finite mass. These are the two factors which define type I behaviour and we will be exploiting them in the time dependent calculations.

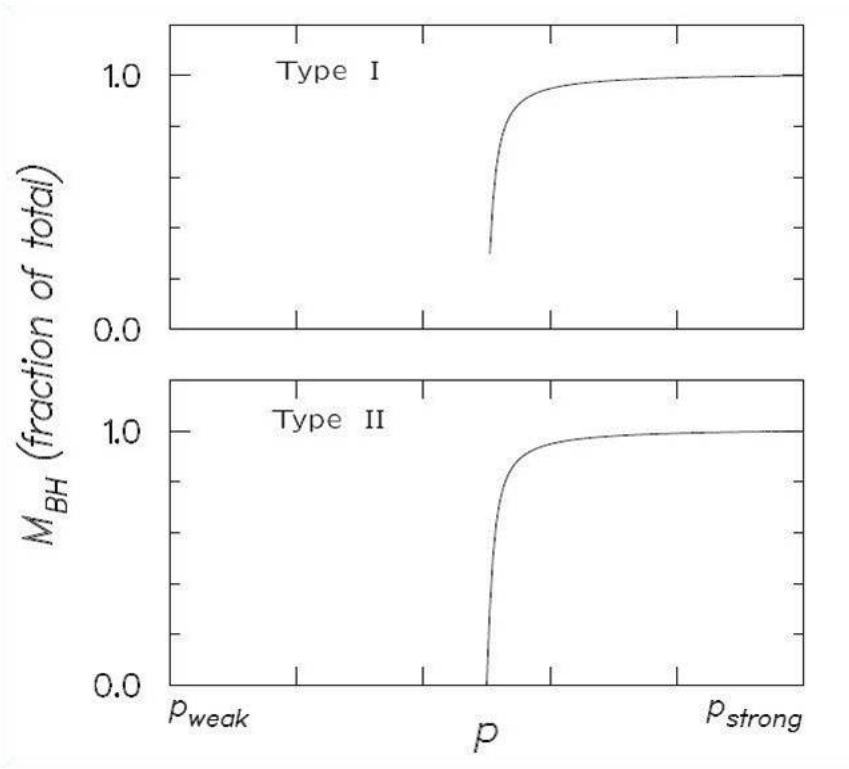

Figure 1.1: These two plots of Mass vs the tuning parameter show that the black hole begin formation at p*(critical value). Type I behaviour, as seen in last years results and expected this year, produces a field which becomes periodic in time. Another feture of Type I collapse is that a finite initial mass is needed to induce blow-up. Type II is not used in this project but displayed for completeness.

Chapter 2

Nonlinear Schrödinger-Poisson System

2.1 Mathemaical Model

Restricting our attention to spherical symmetry we introduce the complex Schrödinger field, $\Psi(r,t)$,

$$\Psi(r,t) = \Psi_1(r,t) + i\Psi_2(r,t) \tag{2.1}$$

where Ψ_1 are Ψ_2 are real fields. The Newtonian gravitational potential will be denoted as $V(r,t)$. Without loss of generality, $c = \hbar = g = 1$, yielding the system of PDEs defined as the Nonlinear Schrödinger-Poisson (NSP)

$$i\frac{\partial \Psi}{\partial t} = -\frac{1}{2}\Delta\Psi + V\Psi \tag{2.2}$$

$$\Delta V = |\Psi|^{\alpha} \qquad 2 \leq \alpha \leq 3 \tag{2.3}$$

Δ will be taken as the laplacian, α is a control parameter which we will use to adjust the strength of the gravitational self-coupling. If we let α=2, the NSP system reduces to the Schrödinger-Poisson (SP) system.

For our purposes, the Schrödinger field, Ψ, typically associated with a single particle in quantum mechanics, is to be viewed as the non-relativistic limit of a classical massive Klein-Gordon field, and thus constitutes a simple model for matter which can self-gravitate. It is important to note here that these calculations are purely classical in the sense that we directly interpret the Ψ field as describing a macroscopic distribution of matter. Ψ evolves according to the Schrödinger equation (2.2), and feels a gravitational potential that is self-generated through the source term $|\Psi|^{\alpha}$ appearing in the Poisson equation (2.3).

2.1.1 Previous work done on this Mathemaical Model

Previous numerical calculations by Andrew Inwood [3] provided strong evidence that there is *no* critical behaviour in the SP system; i.e that irrespective of the nature of the initial data, the subsequent evolution appears to remain singularity free. Inwood studied the dynamical evolution of one-parameter families of initial data for the SP equations, and found that as the family parameter was increased, the resulting solutions appeared to simply be rescaled versions of one

another, so that there was no evidence of focusing or other behaviour that would result in finite-time blowup. The SP system was then modified through the gravitational coupling seen in (2.3), in an attempt to induce critical behaviour. For the specific case of $\alpha = 3$, evidence for Type I critical behaviour was found, with a critical solution that appeared to be periodic.

2.2 Spherical Symmetry

By choosing to work in a spherically symmetric coordinate system, all angular dependency has been eliminated. With this assumption, the laplacian reduces to

$$\Delta f(r) = \frac{1}{r^2}\left(r^2 f'(r)\right)' \tag{2.4}$$

with $f'(r) \equiv \frac{df(r)}{dr}$

2.3 Boundary and Initial Conditions

2.3.1 Boundary Conditions

For both static and time dependent calculations, the following boundary conditions will be enforced. At the inner boundary, we impose that V and Ψ are smooth

$$\frac{dV}{dr}(0,t) = 0 \tag{2.5}$$

$$\frac{d\Psi}{dr}(0,t) = 0 \tag{2.6}$$

The outer boundary conditions are that both V and Ψ go to zero as $r \to \infty$. Since we are implementing numerical analysis, there must be a cut-off, $r_{\max}$, such that all functions go to zero at $r_{\max}$. With this, we let the outer boundary conditions be

$$V(r_{\max}, t) = 0 \tag{2.7}$$

$$\Psi(r_{\max}, t) = 0 \tag{2.8}$$

The advantages to these outer boundary conditions is they are simple to enforce in any numerical scheme. The main disadvantage to this approach is that it limits how long a time over which the equations can be integrated. Because these boundary conditions reflect all incoming waves, if the matter field propagates out to the outer boundary it will reflect and the solution becomes unphysical.

If blow-up is occurring in the model, then the matter will tend to fall into the origin very quickly, and, for sufficiently large $r_{\max}$ a singularity will form before any matter can propagate to the outer boundary [3]. However, this reflective property at the outer boundary condition becomes problematic under certain dispersal conditions and in searching for the critical solution.

2.3.2 Initial Conditions

The initial condition will only be used in the time dependent calculation, and as it will soon be seen, Ψ resembles a gaussian when calculating static solutions. Thus it seems reasionable to choose a gaussian as the initial field.

$$\Psi(r,0) = Ae^{-\frac{r^2}{0.1}} \tag{2.9}$$

Here we have chosen our free parameter for the system to be the aplitute of the gaussian, A. By tuning this parameter, we hope to find the critical solutions of Ψ for the particular α's which allow blow-up to occur.

2.4 Norm calculation

In this paper we will are looking at end behaviour of our system. $|\Psi|^2$ is, as usual, the spatial probability distribution function of the particle; that is, integrating over it tells us the probability of finding the particle in a region of space. Since we are working in spherical symmetry there is an r^2 weighting in the integral; so even if $|\Psi|^2$ is large at the origin, the probability may be small due to this r^2 weighting. Without loss of generality we have chosen to leave $|\Psi|^2$ un-normalized to introduce the conserved quantity I(r)

$$I(r) = \int_o^r s^2 |\Psi(s)|^2 \, ds \tag{2.10}$$

which is proportional to the mass, and will be used to follow the evolution of the mass of our stars. If Ψ is exhibiting blow-up behaviour, then most of the mass is concentrated near the origin and I(r) will exhibit rapid grow for a small value of r. To calculate this integral numerically we employ a Riemann sum using the midpoint rule,

$$I(r_j) = I(r_{j-1}) + dr\left(r_j - \frac{dr}{2}\right)^2 (\Psi_j + \Psi_{j-1})\left(\Psi_j^* - \Psi_{j-1}^*\right) \tag{2.11}$$

with $I(r_1) = 0$, $dr \equiv r_j - r_{j-1}$, and $\Psi^* = conjugate\Psi$

Chapter 3

Relations and Theory of Static Solutions

3.1 Boson Stars

Gravitationally bound and static solutions of the SP system (known as Newtonian boson stars) can be constructed from our system. These solutions correspond to the familiar eigenstates of the 1-d Schrödinger equation in quantum mechanics for the harmonic oscillator; In particular, can be labelled by the number of nodes in the wave functions. The initial part of our work will consider the analogous solutions in the NSP system, with a focus on "'ground state" configurations which have no nodes in their radial profiles, as shown in Fig. 3.1. There are infinitly many boson star solutions, defined by the number of zero crossings. Fig. 3.2 plots the first excited state wavefunction, with each excited state has one more zero than the previous.

3.2 Ansatz of solution and ODE system

To begin our static analysis, we assume solutions of the form

$$\Psi_\alpha(r,t) = e^{i\omega_\alpha t}\Phi_\alpha(r) \tag{3.1}$$

where the subscrpt α denotes the solutions at a fixed α. ω_α are the eigenvalues which correspond to their eigenfunction Φ_α for a given α. When the ansatz given in equation (3.1) is plugged into the NSP system, the time dependency is removed, yeilding the following time independent ODE

$$(r^2\Phi'_\alpha(r))' + r^2(\omega_\alpha - V(r))\Phi_\alpha = 0 \tag{3.2}$$

Figure 3.1: The first bound-state wavefunction (Ψ) is a solution of the time independent SP system. This is a 0 mode solution as (Ψ) does not cross the r-axis before it flattens out, and these are the forms of solutions that we will be analyzing. The solution was calculated by Moroz, Penrose, and Tod [10] numerically using a Runge-Kutta NAG routine (S is a scaled wavefunction)

Figure 3.2: The plot is of the first excited state wavefunction. Each excited state has one more zero than the previous.

$$(r^2V'(r))' = r^2|\Phi_\alpha(r)|^\alpha \tag{3.3}$$

3.2.1 Relate Boson star solutions to Harmonic Oscillator

To my knowledge, equations (3.2) and (3.3) are not analytically solvable, forcing us to use numerical techniques. To show how the eigenvalues (ω_α) affect our eigenfunctions (Φ_α), it is helpful to notice that equation (3.2) is very similar to the 1-d Schrödinger equation with a harmonic oscillator potential.

$$-\frac{\hbar^2}{2m}\frac{d^2\Psi}{dx^2} + \frac{1}{2}m\omega^2x^2\Psi = E\Psi \tag{3.4}$$

With the substitutions $s = \sqrt{\frac{m\omega}{\hbar}}x$ and $K = 2\,\frac{E}{\hbar\omega}$, we get

$$\frac{d^2\Psi}{ds^2} + \left(K - s^2\right)\Psi = 0 \tag{3.5}$$

It is well known that equation (3.5) has the eigenvalues $E_n = (n + \frac{1}{2})\hbar\omega$, and plugging in a given E_n value will produce a normalizable eigenfunction Ψ. However, if $E_n \to E_n \pm \epsilon$ where ϵ is taken to be small, Ψ will diverge to $\pm\infty$. This behaviour is exactly what is seen with the boson star solutions, where Fig. 3.1 and Fig. 3.2 shows the characteristic tail flipping.

Since we cannot obtain exact eigenvalues ω_α for equation (3.2), we will be tuning the tail behaviour of Φ_α to produce ω_α to 16 decimal digits using the "wag-the-dog" method, also known as a binary search.

3.3 Scaling Relations of solutions

Following a scaling relationship described in Choi's Thesis [5], Equations (3.2) and (3.3) have been shown to obey a scaling law relationship that allows all solutions to be calculated from one solution. A slight abuse of notation in this section has replace the α's in Φ_α , V_α, and ω_α by 1, and 2; in reference to the solutions. Consider two solutions labeled by indices 1 and 2, If '1' denotes known solutions to equations (3.2) and (3.3), then

$$\omega_2 = \omega_1\left(\frac{N_2}{N_1}\right)^2 \tag{3.6}$$

$$r_2 = r_1\left(\frac{N_1}{N_2}\right)^{\left(\frac{1}{\alpha-1}\right)} \tag{3.7}$$

$$\Phi_2 = \Phi_1\left(\frac{N_2}{N_1}\right)^{\left(\frac{2}{\alpha-1}\right)} \tag{3.8}$$

$$V_2 = V_1\left(\frac{N_2}{N_1}\right)^{2} \tag{3.9}$$

'2' will be solutions of the same equations, where N is the conserved particle number defined as $N = \int r^2\Phi^2 dr$.

To see this relationship, assume that solutions '2' satisfy equations (3.2) and (3.3),

$$\frac{1}{2r_2^2}\frac{d}{dr_2}\left(r_2^2\frac{d}{dr_2}\Phi_2\right) + (\omega_2 - V_2)\,\Phi_2 = 0 \tag{3.10}$$

$$\frac{1}{r_2^2}\frac{d}{dr_2}\left(r_2^2\frac{d}{dr_2}V_2\right) = \Phi_2^\alpha \tag{3.11}$$

Applying the scaling relations from (3.6), (3.7), (3.8), and (3.9), we get

$$\left(\frac{1}{2r_1^2}\frac{d}{dr_1}\left(r_1^2\frac{d}{dr_1}\Phi_1\right) + (\omega_1 - V_1)\,\Phi_2\right)\left(\frac{N_2}{N_1}\right)^{\left(\frac{4}{\alpha-1}\right)} = 0 \tag{3.12}$$

$$\frac{1}{r_1^2}\frac{d}{dr_1}\left(r_1^2\frac{d}{dr_1}V_1\right)\left(\frac{N_2}{N_1}\right)^{\left(\frac{2\alpha}{\alpha-1}\right)} = \Phi_2^\alpha\left(\frac{N_2}{N_1}\right)^{\left(\frac{2\alpha}{\alpha-1}\right)} \tag{3.13}$$

where it can be seen this relationship works for all α's.

3.4 Integral relations between $\Phi_\alpha(r)$ and $V_\alpha(r)$

Three integral relationships between $\Phi_\alpha(r)$ and $V_\alpha(r)$ can be extracted from equations (3.2) and (3.3) by multiplying the equations with a function and integrating over all space.

1) Multiply equation (3.2) by $\Phi_\alpha(r)$ and integrate over all space

$$\int_0^\infty \Phi_\alpha\left(r^2\Phi_\alpha'\right)' dr = \int_0^\infty r^2\left(V_\alpha - \omega_\alpha\right)\Phi_\alpha^2 dr \tag{3.14}$$

And integrate the left hand side by parts, noticing the boundary terms are zero, we are left with the relationship

$$\int_0^\infty r^2 \left((V_\alpha - \omega_\alpha) \Phi_\alpha^2 + \left(\Phi_\alpha'\right)^2 \right) dr = 0 \tag{3.15}$$

2) Multiply equation (3.3) by $V_\alpha(r)$ and integrate over all space

$$\int_0^\infty V_\alpha \left(r^2 V_\alpha'\right)' dr = \int_0^\infty r^2 V_\alpha \Phi_\alpha^\alpha dr \tag{3.16}$$

And integrate the left hand side by parts, noticing the boundary terms are zero, we are left with the relationship

$$\int_0^\infty r^2 \left(V_\alpha \Phi_\alpha^\alpha + \left(V_\alpha'\right)^2 \right) dr = 0 \tag{3.17}$$

3) Multiply equation (3.2) by $V_\alpha(r)$ and (3.3) by $\Phi_\alpha(r)$. Subtract the two functions and integrate over all space

$$\int_0^\infty \left(V_\alpha \left(r^2 \Phi_\alpha'\right)' - \Phi_\alpha \left(r^2 V_\alpha'\right)' \right) dr = \int_0^\infty r^2 \left(V_\alpha \left(V_\alpha - \omega_\alpha\right) \Phi_\alpha - \Phi_\alpha^{\alpha+1} \right) dr \tag{3.18}$$

Where again, we can simplify by integrating by parts and throw away the boundary terms, yielding

$$\int_0^\infty r^2 \left(V_\alpha \Phi_\alpha \left(V_\alpha - \omega_\alpha\right) - \Phi_\alpha^{\alpha+1} \right) dr = 0 \tag{3.19}$$

Equations (3.15), (3.17), and (3.19) have been written in the form $\int_0^\infty r^2 f(r) dr = 0$. These relationships have been included to show the relationships between Φ_α and V_α; However, I will not explore them further.

3.5 Validity of r_{max} in static settings

In future calculations, the solutions for Φ_α will been croped to create a numerically integrable function. It is desired that our numerical approximation of Φ_α integrates reasionably close to the true value. The spacial probability can be written as

$$\int_0^\infty r^2 \Phi_\alpha^2 = \int_0^{r_{max}} r^2 \Phi_\alpha^2 + \int_{r_{max}}^\infty r^2 \Phi_\alpha^2 \tag{3.20}$$

Further, from [1] we know that Φ_α has an exponential tail, so it is valid to make the approximation

$$\int_0^{\infty} r^2 \Phi_\alpha^2 \simeq \int_0^{r_{max}} r^2 \Phi_\alpha^2 + \int_{r_{max}}^{\infty} r^2 (Ae^{-r})^2 \tag{3.21}$$

Where Φ_α has been replaced with Ae^{-r}; A is on the order of 10^{-5} (the typical values for $\Phi_\alpha(r_{max})$) to enforce continuity between Φ_α and e^{-r} at $r = r_{max}$. The last term in equation (3.21) can be easily integrated, yielding

$$\int_{r_{max}}^{\infty} r^2 (Ae^{-r})^2 = \frac{A^2}{4} \left(1 + 2\, r_{\max} + 2\, {r_{\max}}^2\right) \mathrm{e}^{-2\, r_{\max}} \tag{3.22}$$

For the work to follow, $r_{max} \geq 10$, plugging into (3.22)

$$\int_{r_{max}}^{\infty} r^2 (Ae^{-r})^2 \leq 10^{-7} A^2 \tag{3.23}$$

which shows our numerical scheme will provide accuracy of the integral on the order of $10^{-7}A^2$, where A is on the order of 10^{-5}.

Chapter 4

Numerical analysis of Static Solutions

4.1 Calculating Solutions of ODE system

Equations (3.2) and (3.3) can be solved using a forward integration starting at r=0, and implementing a technique called "shooting"; so the solution satisfies the boundary conditions at $r = r_{\max}$. One expects the solutions to be parametrized by the central value $\Phi_\alpha(0)$ which, naively, leaves two shooting parameters, $V(0)$, and the eigenvalue ω_α.

We can in fact choose $V(0) = 0$ (or any other constant) and then adjust ω_α until $\Phi_\alpha(r_{max}) \to 0$. We then have a solution $\Phi_\alpha(r)$ and $V(r; \Phi_\alpha(0))$ but where $V(r; \Phi_\alpha(0))$ does not go to 0 as $r \to \infty$. However, if $V(r)$ is a solution to (3.2) then so is $V(r) + c$ where c is an arbitrary constant. Thus, to get a solution that satisfies both boundary conditions as $r \to \infty$ we need only take $V(r; \Phi_\alpha(0)) \to V(r; \Phi_\alpha(0)) + c$ and $\omega_\alpha \to \omega_\alpha + c$ where c is chosen so that $V \to 0$ as $r \to \infty$.

4.2 Eigenvalues

Equations (3.2) and (3.3) form an eigenvalue problem, where Φ_α are the eigenfunctions of the corresponding eigenvalues ω_α. As previously discussed, there are infinitly many Φ_α solutions to equations (3.2) and (3.3); however only one stable solution (no zero crossing). Numerically it is easier and more accurate to first calculate Φ_α and ω_α with the initial condition $V_\alpha(0) = 0$, and then perform the shifts described in section 'Calculating Solutions of ODE system'

Firstly, looking at the eigenvalues before the shifts; A trend has appeared showning that the the eigenvalues can be listed $\omega_{\alpha 0} < \omega_{\alpha 1} < \omega_{\alpha 2} < ...$, where $\omega_{\alpha 0}$ corresponds to the stable solutions, and $\omega_{\alpha i}$ corresponds to the i^{th} excited state (i zero crossings in the eigenfuction $\Phi_{\alpha i}$)

Further, looking at the first mode stable eigenvalues, and plotting ω_α against the initial condition $\Phi_\alpha(0)$; a relationship between α, ω_α, and $\Phi_\alpha(0)$ has been found.

$$\omega_\alpha = C\Phi_\alpha(0)^{\frac{\alpha}{2}} \tag{4.1}$$

where the constant 'C' has the property that the eigenvalues have the same value when $\Phi_\alpha(0) \simeq 1.2248$, and can be seen in Fig. 4.1. These eigenvalues are accurate to 16 decimal places. However, up to now, the gravitational field has been given the initial condition $V(0)$, which gives the wrong asymptotic behaviour. The true eigenvalues are more sensitive to calculate, and can be seen on Fig. 4.2

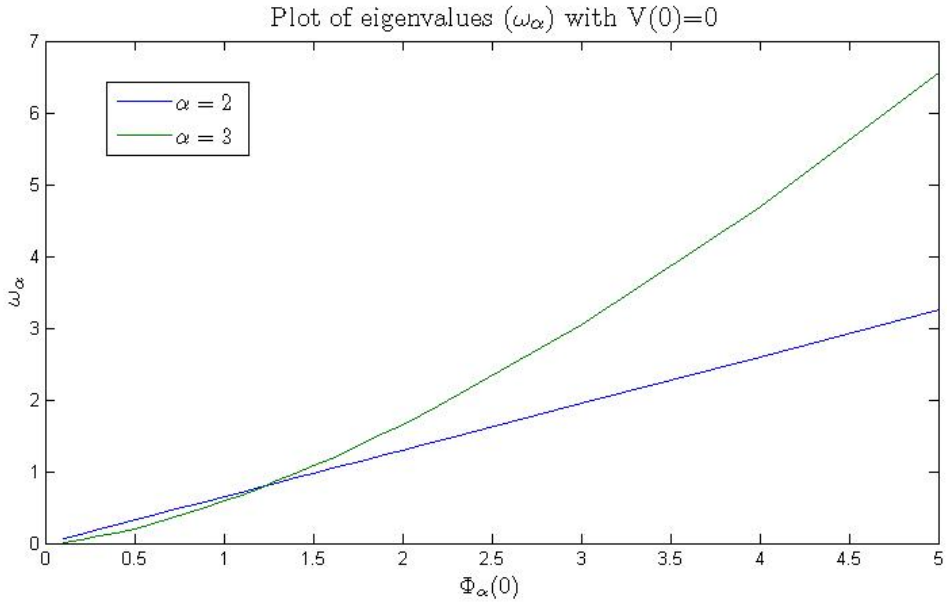

Figure 4.1: This plot shows the relationship between the eigenvalues (ω_α), initial condition of the eigenfunctions ($\Phi_\alpha(0)$), for $\alpha = 2$ and $\alpha = 3$ with $V(0) = 0$

It can be seen through Fig. 4.5 that by shifting ω_α and $V(0)$ to get the correct asymptotic behaviour for $V(r)$, that Φ_α is unchanged, and the accuracy (length that Φ_α is valid) has been reduced by half. Thus, all following calculations will use eigenvalues and eigenfunctions with the initial condition $V(0) = 0$, since we are not looking at the gravitational field in any static calculations.

4.3 Eigenfunctions

Our eigenfunctions, Φ_α, have the behaviour of a monotonically decreasing function which are always greater than or equal to zero. Once coded in Matlab, it was found that when Φ_α increases ω_α needed to be decreased; and when Φ_α was less than zero, ω_α needed to be increases to maintain correct end behaviour. A loop was then made repeating these calculations until ω_α was known to 16 decimal places. Solution curves to our coupled ODE system can now be produced as shown in Fig. 4.3.

With our solution know for any α, we will now create an r_{max} for all solutions to cut off the "tail" as seen in Fig. 4.3. Φ_α monotonically decreases to zero, before it wildly explodes to $\pm\infty$. Thus, r_{max} has been defined as the point where the absolute value of $\frac{d\Phi}{dr}$ is minimum (away from the origin). The typical values of $\Phi(r_{max})$ are on the order of 10^{-5}.

Once we have cropped our solutions, $\Phi_\alpha(r)$ and $V_\alpha(r)$ take the form of Fig.4.4. It can be seen that the solutions drop off quickly for large $\Phi_2(0)$, while small $\Phi_2(0)$ produce flatter solutions.

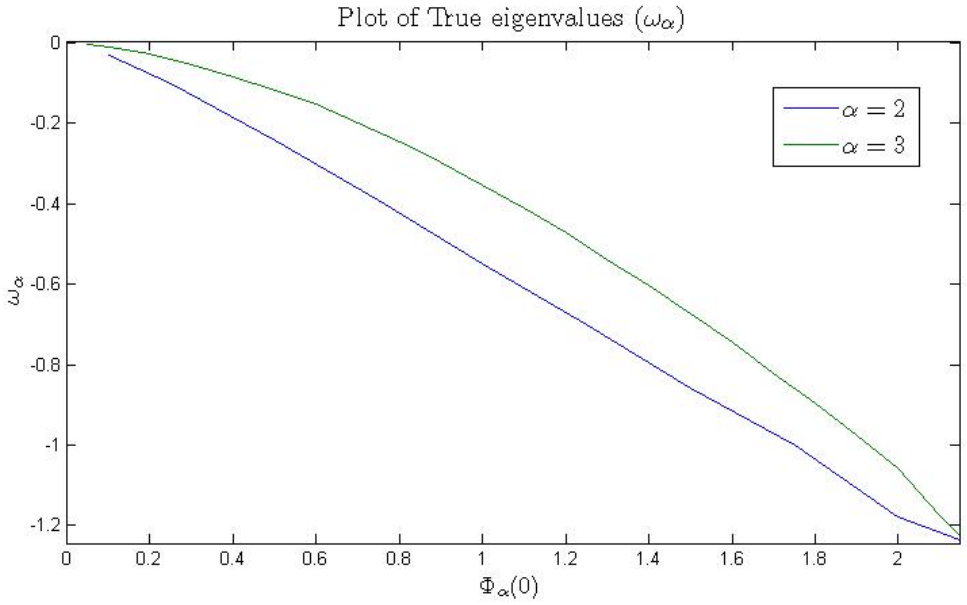

Figure 4.2: This plot shows the true relationship between the eigenvalues (ω_α), initial condition of the eigenfunctions ($\Phi_\alpha(0)$), for $\alpha = 2$ and $\alpha = 3$. Now $V(r_{max}) = 0$, giving the correct behaviour for the gravitational field

This behaviour is consistent for $2 < \alpha \leq 3$.

4.4 Results

We now have $\Phi_\alpha(r)$ as a monotonically decreasing integrable function, which can be found for and α and $\Phi_\alpha(0)$, we are in a position to look at some properties of our system. To begin, we chose to look at the conserved quantity

$$\aleph(\alpha, \Phi_\alpha(0)) = \int_0^\infty \Phi_\alpha^2(r) r^2 dr \tag{4.2}$$

which is propotional to the mass of our system, Without loss of generality,

$$\aleph(\alpha, \Phi_\alpha(0)) = \int_0^{r_{max}} \Phi_\alpha^2(r) r^2 dr \tag{4.3}$$

The initial condition $\Phi_\alpha(0)$ can be viewed as characterizing the central pressure of the configuration, and α is the gravitational strength. This has been done to try and understand how, and why α and pressure influences the mass of our system.

Fig. 4.6 shows the plots (mass vs central pressure) of our three extremes for static solutions in our range $2 \leq \alpha \leq 3$. For α=2, it was found that mass is proportional to central density; The mass of system ($\aleph$) grows with the central density ($\Phi_\alpha(0)$) with the relation $\aleph$=2.06$(\Phi_2(0))^{0.5}$.

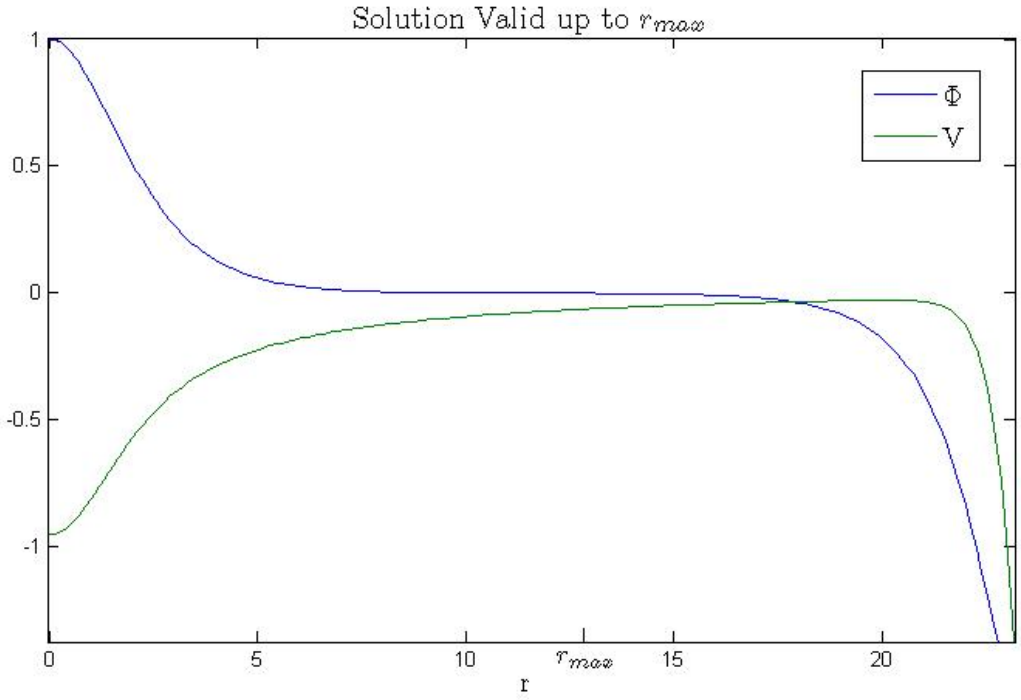

Figure 4.3: This plot shows $\Phi_\alpha(r)$ and V(r) with machine precision of the eigenvalue ω_α. Our solutions are valid up to $r = r_{max}$; After that point, the exponential decay behaviour is replaced by a diverging solution. The divergence behaviour seen for $r > r_{max}$ is purely a numerical phenomenon controlled by the eigenvalues.

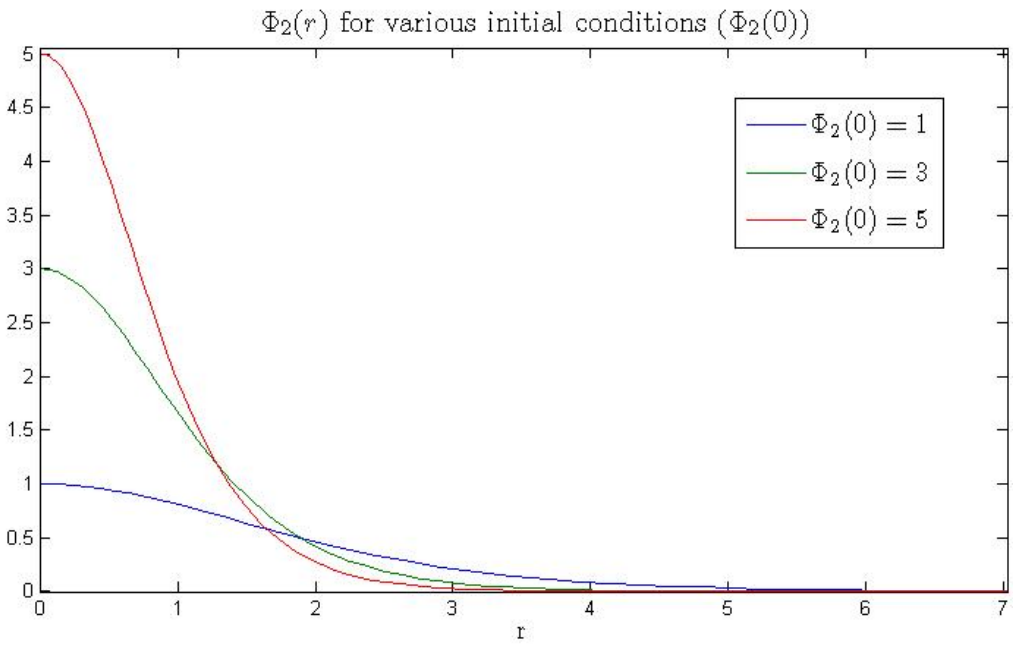

Figure 4.4: $\Phi_2(r)$ are the static solutions of the NSP system for various initial conditions $\Phi_2(0)$. The higher $\Phi_2(0)$ is, the steeper $\Phi_2(r)$ drops off to zero. This same behaviour is noticed for $\alpha = 3$. These solutions have been plotted up to r=7 to see behaviour near origin; however, $r_{max} = 18$ for $\Phi_2(0) = 5$ and $r_{max} = 44$ for $\Phi_2(0) = 1$

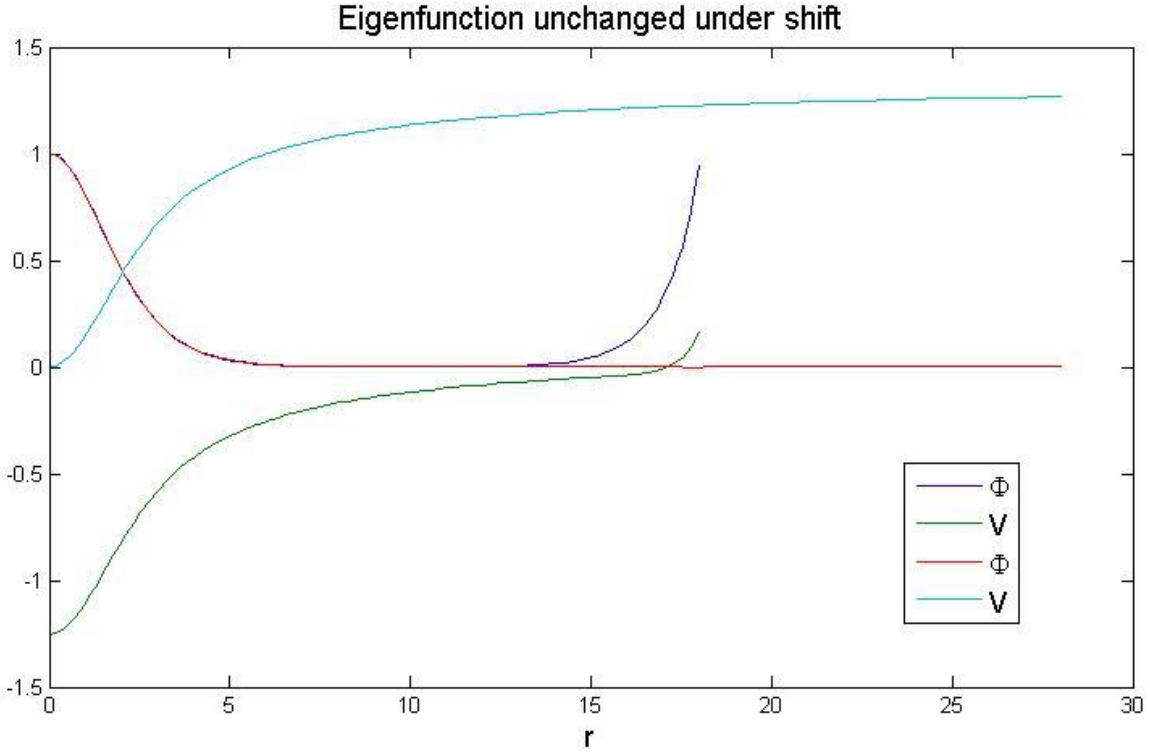

Figure 4.5: This plot shows by shifting ω_α and $V(0)$ to get the correct asymptotic behaviour for $V(r)$, that Φ_α is unchanged, and the accuracy (length that Φ_α is valid) has been reduced by half

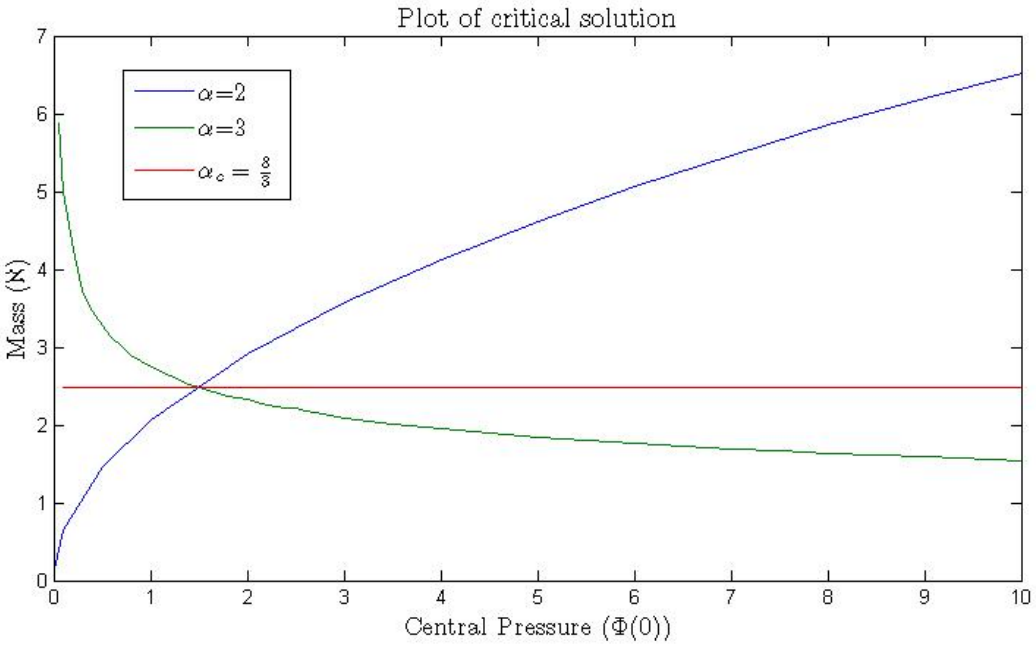

Figure 4.6: Plot of $\aleph(\alpha, \Phi_\alpha(0))$ dr vs $\Phi_\alpha(0)$ to see how mass of system is ($\aleph$) affected by changing the gravitational coupling given initial conditions of central density $\Phi_\alpha(0)$. The critical solution (with $\alpha = \frac{8}{3}$) was found using a binary search between monotonically increasing and decreasing $\aleph(\Phi_\alpha(0), \alpha)$

This type of behavior shows the static solution is stable.

However, when we increase the strength of the gravitational coupling to $\alpha = 3$, Fig. 4.6 shows that mass is inversely proportional to central pressure. This behaviour suggests blow-up occurs, as mass grows unbounded with a decreasing central pressure. It was found that $\aleph = 2.75(\Phi_3(0))^{-0.25}$, which we believe corresponds to 1 mode unstable static solutions.

Since we are interested in the critical solution, that is exactly where this behaviour changes, a binary search was implemented to find the boundary of these two behaviours. We found that there was a constant solution for $\alpha \simeq \frac{8}{3}$ (denoted α_c), that is mass is constant for all initial central pressures as shown in Fig. 4.6.

It can be seen that $\aleph \propto (\Phi_\alpha(0))^x$ where $x(\alpha)$. This is a simple linear relation, showing $x(\alpha) = -\frac{3}{4}\alpha + 2$, thus

$$\aleph(\Phi_\alpha(0), \alpha) \propto (\Phi_\alpha(0))^{-\frac{3}{4}\alpha+2} \tag{4.4}$$

The relationship described in equation (4.4) completely defines our system in terms of the physical quantities mass and central density. The next job looking at the stability of our solutions in these different regions to get a better understanding of why this relationship occurs.

Chapter 5

Static Stability Analysis

5.1 Introduction to stability analysis

In this chapter, stability analysis will be done by introducing a small pertubation in our fields. Physically, introducing this pertubation corresponds to introducing a small disturbance in a "perfectly stable" star. Once this pertubation is introduced, the star can either absorb and restabalize or become unstable. We can determine which solutions are stable or unstable by looking to see if the perturbations are oscillatory or exponentially growing in time.

Results from last years research has given strong evidence that $\alpha = 2$ produces stable solutions, and $\alpha = 3$ produces 1-mode unstable solutions. Static analysis has found the relationship through equation (4.4) defining how the mass behaves for different α's. Combinding the above facts, the following conjectures will be made:

- $2 \leq \alpha < \alpha_c$ the static solutions are all stable
- $\alpha_c < \alpha \leq 3$ static solutions are all 1-mode unstable

At this point, their have been no clues to the stability of $\alpha = \alpha_c$; And further investigation is required.

5.2 Defining Pertubations

To begin, we will use the same ansatz for the wavefunction as equation (3.1), and add a small pertubation in the fields.

$$\Psi(r,t) = e^{-iwt}\Phi(r) + \epsilon\, e^{-iw_\epsilon t}\Phi_\epsilon(r) \tag{5.1}$$

$$V_{total}(r) = V(r) + \epsilon\, V_\epsilon(r) \tag{5.2}$$

Here we have introduces an O(ϵ) pertubation into both of the fields. ω_ϵ are the eigenvalues corresponding to the eigenfunctions Φ_ϵ in the perturbed field. There will also be a V_ϵ introduced in the gravitational field to composate for Φ_ϵ.

To look for exponential behaviour in our fields, it is natural to let the eigenvalues be complex, w_ϵ=a+ib. Plugging this into equation (5.1) we get

$$\Psi(r,t) = e^{-iwt}\Phi(r) + \epsilon\, e^{-iat}e^{bt}\Phi_\epsilon(r) \tag{5.3}$$

where it can be seen that e^{bt} will determine our stability; yielding the three conditions on b for stability:

- b>0 produces exponential growth in time, 1-mode unstable
- b=0 will provide no information
- b<0 produces exponential decay which quickly eliminates the pertubation, 1-mode stable

5.3 Calculations

Plugging equations (5.1) and (5.2) into the NSP system, we obtain two coupled O(1) and two coupled O(ϵ) equations. Our O(1) equations are the same as equations (3.2) and (3.3). The O(ϵ) equations are

$$(r^2\Phi_\epsilon'(r))' + r^2(w_\epsilon - V(r))\Phi_\epsilon(r) + 2r^2V_\epsilon(r)\Phi(r) = 0 \tag{5.4}$$

$$(r^2V_\epsilon'(r))' = r^2|\Phi_\epsilon(r)|^\alpha \tag{5.5}$$

These ODE's are not analytically (as far as i know) solvable, so MATLAB will be implemented to numerically solve equations (3.2), (3.3), (5.4) and (5.5).

These solutions have been solved in a two step process. Firstly the O(1) solutions were found using methods described in previous section as they have no dependency on the O(ϵ) equations. Secondly, the O(ϵ) equations were numerically solved. This process required two shooting parameres as we require Φ_ϵ and V_ϵ to go to zero as $r \to r_{\max}$. Φ_ϵ is the eigenvalue controlled by its eigenvalue ω_ϵ and was found using a binary search. Once Φ_ϵ was found, V_ϵ which initially had the boundary condition $V_\epsilon(0)$=0 was simply shifted down through trial and error until $V_\epsilon(r_{max}) = 0$

Fig. 5.1 has been plotted showing the solution curves for Φ, Φ_ϵ, V, and V_ϵ. It can be seen that the perturbed field Φ_ϵ has been given the same initial conditions as Φ.

5.4 Results

I began my calculations with α=2, and found that ω_ϵ was purely real, yeilding no information. I then checked $\alpha = 3$ where critical behaviour was found last year and $\alpha = \frac{8}{3}$, where static solutions suggest we have a critical solution in the NSL system. Both of these results yielded b=0, forcing us to make the conclusion that static pertubations on our system provide no information on the

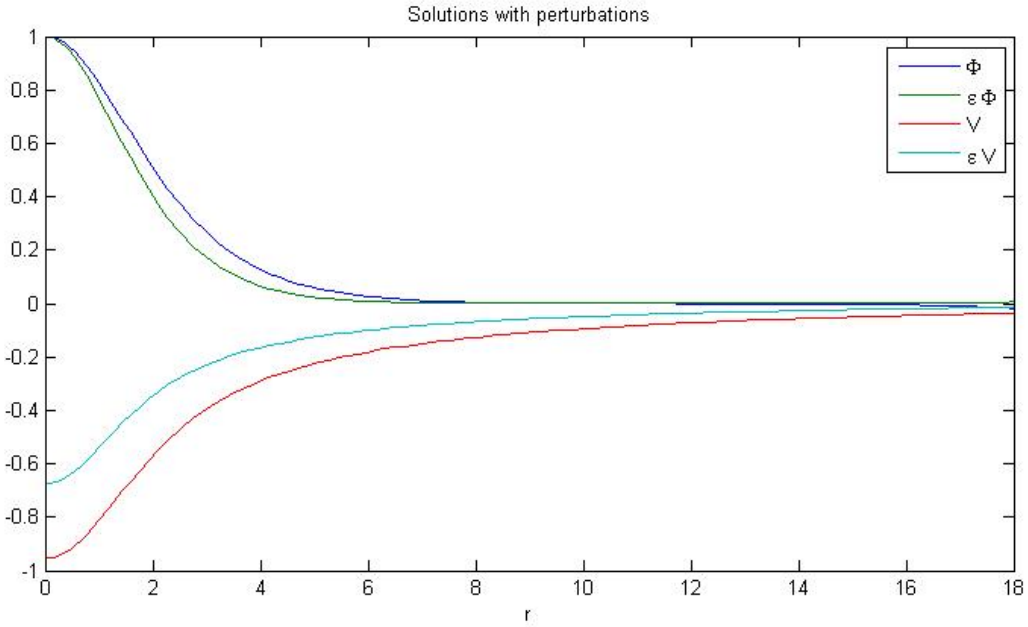

Figure 5.1: This plot shows Φ, Φ_ϵ, V, and V_ϵ solved with ω, and ω_ϵ accurate to machine precision.

stability of the NSP system. Fortunatly not all is lost, this just means that we are going to have to look at the more complecated time dependent stability cases discussed in the next two chapters.

Chapter 6

Time Dependent Analysis using Matlab

6.1 Code

I began The time dependent analysis using a pre-programed matlab code called PDEPE. This program requires three seperate files: boundary conditions, initial conditions, and the equations. The mesh for the spacial component was chosen to be:

$$x\left(i\right) = R\left(1 - \cos\left(\frac{i\pi}{2N}\right)\right) \tag{6.1}$$

where i indexes from 1 to N, and N is the number of spacial mesh points. This mesh was chosen over a uniform mesh because we are looking for blow-up, which occurs at the origin. So the natural choice is to choose a mesh which smoothly consitrates at the origin. The spacial mesh is automatically chosen by PDEPE to be uniform.

6.2 Confirm last years results

6.2.1 NSP system with $\alpha = 2$

Beginning with $\alpha = 2$ in the NSP system, last years results suggested that blow-up could not be induced.

This system was studied extensively last year by Inwoods, and all results indicated a system that does not support blow-up. Fig. 6.2 shows the time derivative of mass near the origin. It can be seen that increasing A increases the initial growth, however, dispursal always occurs. Inwoods found that there was a scaling relationship between Ψ and A [**?**].

It has been found that the dispersal of Ψ in this region takes two forms. Under low A values, the field does not have the gravitational strength for any growth, and dispersal is imediate as shown in Fig. 6.1. A little more interesting, is when the initial gaussian gives the system enough mass for growth. However, as previously mentioned, Ψ will never collapse at the origin because the gravitational strength will not support such behaviour.

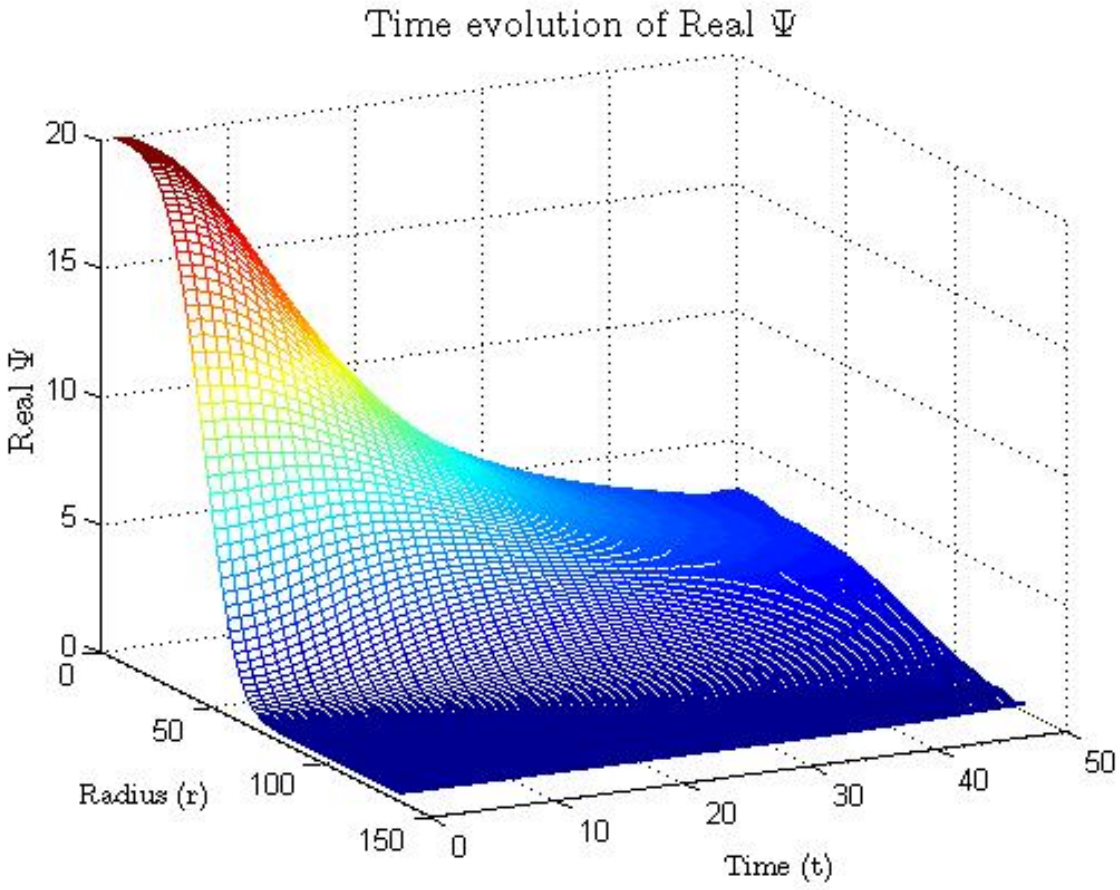

Figure 6.1: This plot shows the dispersal of Ψ which would result under week gravity or low amplitude (A)

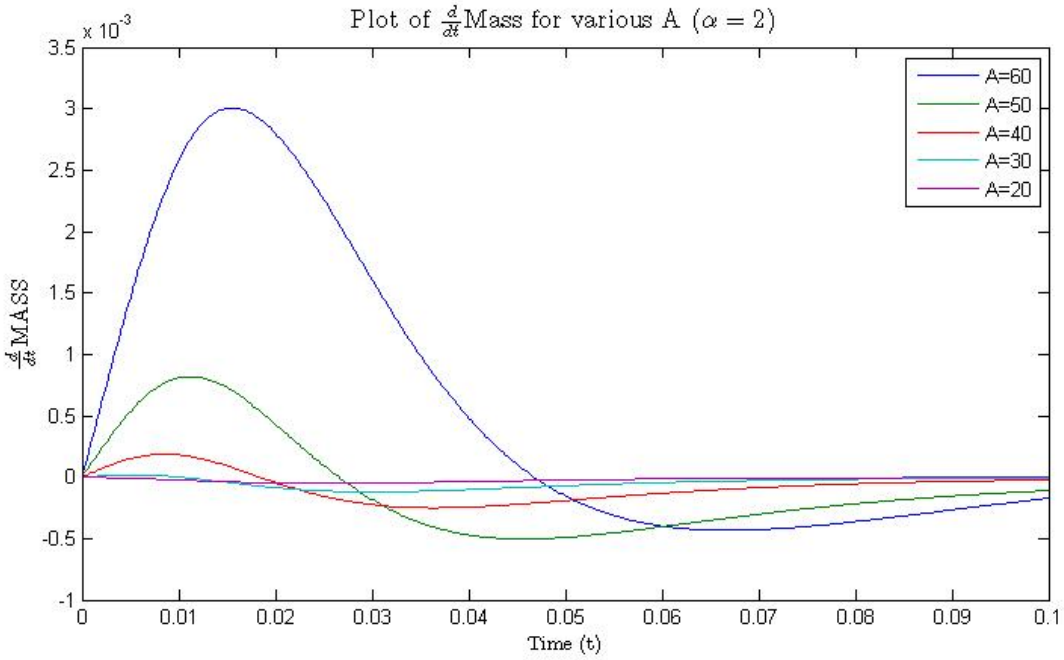

Figure 6.2: Setting $\alpha = 2$ in the MSP system, we see initial growth in the mass at the origin followed by dispersion, indicating that the gravitational strenth is not strong enough to hold the system together. There is also evidence that the MSP system scales in time with A as the growth rates of the mass exhibit similar behaviour on different time scales.

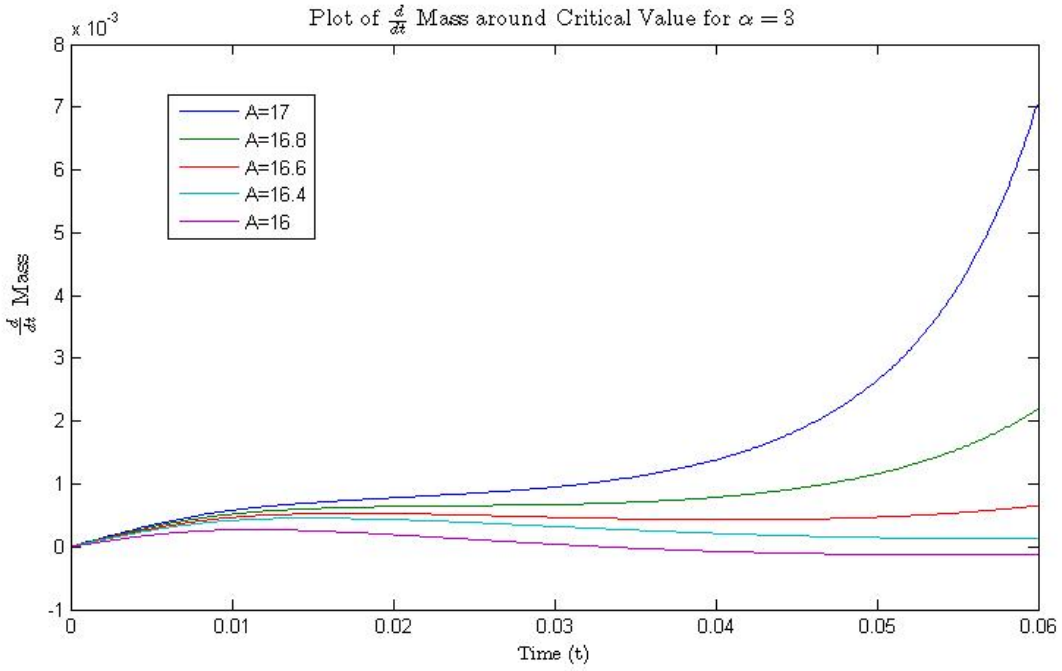

Figure 6.3: Setting $\alpha = 3$ in the MSP system, two distinctly different behaviours are noticed. For $0 < A < 16$, the mass shows same behaviour as seen with α=2. For $16 < A < 17$ this plot shows the transition between the dispersal and blow-up states. And for $A > 17$ blow-up time decreases as A increases

6.2.2 NSP system with $\alpha = 3$

The second extreme of our system is setting $\alpha = 3$ in the NSP system, where blow-up has been found to occur. Two distinctly different behaviours occur with the central mass of the system which can be seen in Fig. 6.3. Setting the amplitude within the region $0 < A < 16$ yields the same behaviour that was seen for $\alpha = 2$; Their is either complete dispersal or some initial growth followed by quick dispersal. However, this region is dispersing for a different reason than seen in the $\alpha = 2$ case. Here, it is the fact that we are not giving enough mass into our system to induce blow-up.

Fig. 6.3 has been plotted showing how a small mass increase in our system (controlled by A) will produce drastically different results. Somewhere in the region $16 < A < 17$, Ψ has switched its behaviour from dispersal to 'blow-up'. Fig. 6.4 shows the evolution of Ψ, characteristic of 'blow-up'.

The NSP system with $\alpha = 3$ has demonstrated that blow-up occurs in the NSP. The goal at this point is to tune 'A' to machine percision for all α's that allow blow-up to occur; Then look at the critical solution of Ψ and perform stability analysis.

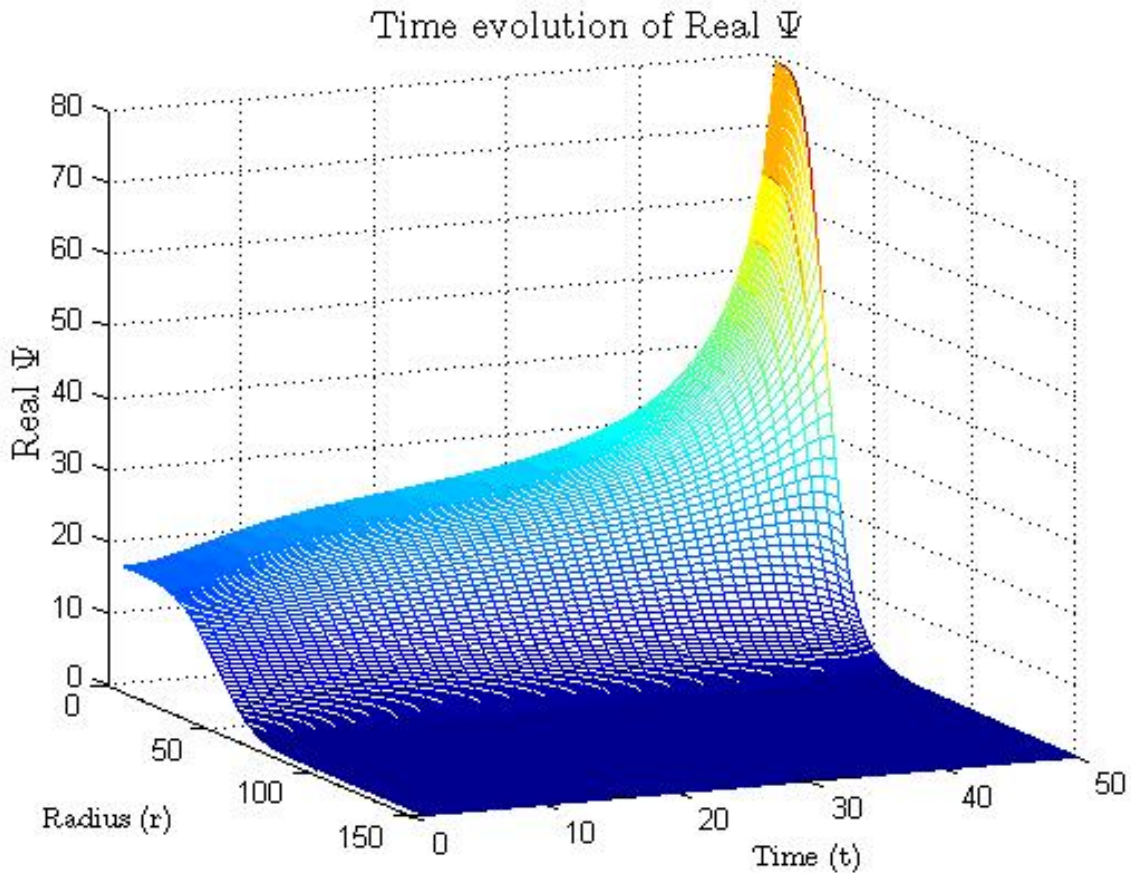

Figure 6.4: This plot shows the exponential growth of Ψ. This plot was taken with $\alpha = 3$, and A=16, which is just under the critical solution.

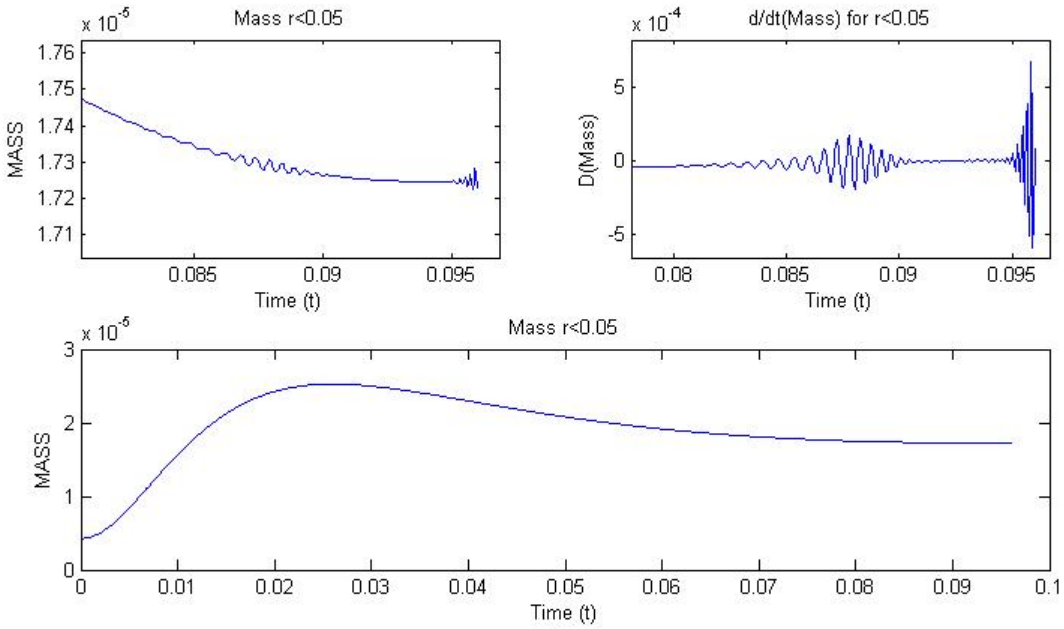

Figure 6.5: In tuning 'A' to produce the critical value ($\Psi_{critical}$), it can be seen that fluxuations are occuring at the origin. These fluxuations are due to Ψ propogating to the outer boundary and back to the origin. The fluxuations can be removed by increasing r_{max}, at the cost of computational power.

6.3 Results and limitations

It has been demonstrated by Fig. 6.3 that our critical value of 'A' will lie in the region $16 < A < 17$ for $\alpha = 3$.

In looking for a critical solution, It was helpful to follow the Mass of the system near the origin. As the critical solution is the threshold of blackhole formation, the mass with neither grow or decay. Unfortunatly, Matlab was not able to resolve 'A' to more than two decimal places. The problem was that by increasing the accuracy of 'A', we were increases the time we must look at our solution. Increasing the time presents the problem that our solution has time to propogate to the outer boundary and reflect back into the origin. To composate for the boundary reflections, the spacial domain was increased. It was found that memory became an issue and it was not feasable to find critical solutions using Matlab. Fig. 6.5 has been included to show the fluxuations that occur from Ψ propogating to the outer boundary and back to the origin when looking for the critical solution.

Chapter 7

Time Dependent Analysis using a Finite Difference Approximation

Due to limitations of Matlab in calculating critical solutions, Code written by Andrew Inwoods has been implemented. A brief outline of the discretization and code will be summarized here; However, for a full derivation please refer to Inwoods thesis [3].

7.1 Discretization

7.1.1 Spacial and Temral points

Fig. 7.1 displays how our spacial and tempral domains will be discretized. subscripts will indicate the spatial point, and superscripts will indicate the time level. h and dr will be used synonymously to describe the spacing of the spatial coordinate, and the time spacing is set to be proportional to h, The proportionality constant λ is known as the Courant factor, such that.

$$\lambda = \frac{dt}{dr} \tag{7.1}$$

The spacial domain will be denoted r_j, with j=1,2,...,N. We will also use half steps, defined as

$$r_{j\pm\frac{1}{2}} = r_j \pm \frac{h}{2} \tag{7.2}$$

which will be needed to satisfy our accuracy as described in the next section.

7.1.2 NSP System

All calculations will be carried out to O(h^2) accuracy. The descritization of the NSP will be done by breaking the system down several components, and combinding them together.

Figure 7.1: This figure shows the discretization of our spacian and tempral domains. Subscripts will indicate the spatial point and superscripts will indicate the time level . The mesh spacing for the spacial points is denoted h. λ will be set to $\frac{1}{2}$ to implement a Crank-Nicolson scheme, centering the tempral points at the half time level, denoted with the red dots.

The time derivitive which shows up in the Schrödinger equation will be descretized into half time steps ($\lambda = \frac{1}{2}$) to satisfy the accuracy requirements, those steps are displayed in Fig. 7.1 and the derivitive becomes

$$\left(\frac{\partial \Psi}{\partial t}\right)_j^{n+\frac{1}{2}} = \frac{{\Psi_j}^{n+1} - {\Psi_j}^n}{dt} \tag{7.3}$$

Smoothness at the origin is best enforced by our numerical scheme if the The laplacian is written in terms of r^3

$$\Delta f = 3\frac{\partial}{\partial r^3}\left(r^2 \frac{\partial f}{\partial r^3}\right) \tag{7.4}$$

And by implementing the half spacial points, the laplacian becomes

$$\Delta f = 3\left(\frac{{r_{j+\frac{1}{2}}}^2 (f_{j+1} - f_j)}{dr} - \frac{{r_{j-\frac{1}{2}}}^2 (f_j - f_{j-1})}{dr}\right)\left({r_{j+\frac{1}{2}}}^3 - {r_{j-\frac{1}{2}}}^3\right)^{-1} \tag{7.5}$$

With our laplacian and time derivitive as written above, we are able to write the FDA Schrödinger equation as

$$\begin{aligned}\frac{i\left({\Psi_j}^{n+1} - {\Psi_j}^n\right)}{dt} \quad = \quad & -\frac{3}{2\left({r_{j+\frac{1}{2}}}^3 - {r_{j-\frac{1}{2}}}^3\right)}\left[\frac{{r_{j+\frac{1}{2}}}^2\left({\Psi_{j+1}}^{n+1} - {\Psi_j}^{n+1} + {\Psi_{j+1}}^n - {\Psi_j}^n\right)}{2dr}\right. \\ & \left. -\frac{{r_{j+\frac{1}{2}}}^2\left({\Psi_{j+1}}^{n+1} - {\Psi_j}^{n+1} + {\Psi_{j+1}}^n - {\Psi_j}^n\right)}{2dr} + \left({V_j}^{n+1}{\Psi_j}^{n+1} + {V_j}^n{\Psi_j}^n\right)\right.\end{aligned} \tag{7.7}$$

and the FDA Poisson equation is

$$3\frac{\left(r_{j+\frac{1}{2}}\left(\frac{V_{j+1}^n - V_j^n}{dr}\right)\right)^2 - \left(r_{j-\frac{1}{2}}\left(\frac{V_j^n - V_{j-1}^n}{dr}\right)\right)^2}{\left(r^3_{j+\frac{1}{2}} - r^3_{j-\frac{1}{2}}\right)} = \left|\Psi_j^n\right|^\alpha \tag{7.8}$$

7.1.3 Code

Inwoods developed all of the machinery to take an initial state Ψ^1 and calculate the state at the next time level Ψ^2, while satisfying the NSP system and boundary conditions. Routines have been developed to quickly and efficiently invert tridiagonal matrices, and we use the routines found in LAPACK for tridiagonal matrices: DGTSV and ZGTSV. A skeleton code for solving

the NSP system is written in RNPL (Rapid Numerical Prototyping Language), and the updates are written in FORTRAN 77

For more details please refer to Andrew Inwoods Thesis [3].

7.2 Introduction to stability analysis

The following data will be generated using the Finite Difference Approximation with RNPL, followed by analysis through Matlab.

The two regions of interest are $\alpha = \alpha_c$ and α=3. We will be using the smoothness of our NSP system found in the static case and displayed in equation (4.4) to assume that $\alpha < \alpha_c$ behaves the same as $\alpha = 2$ and $\alpha > \alpha_c$ behaves the same as $\alpha = 3$. α=3 is expexted to be 1-mode unstable, at blow up was found in last years results and has been confirmed. $\alpha = \alpha_c$ will produce the most interesting results, as this is critical value for the NSP system, which in essence carries two critical values, α_c and potentially a critical amplitude A.

To begin our look for the stability of the NSP, we must first find the critical amplitude for a given α. Once $A_{critical}$ has been found to 16 decimal places by performing a binary search, the critical solution will give us the information about stability. As discussed earlier, our critical solutions in this system are Type 1, which have been shown to oscillate in time; increasing the accuracy of $A_{critical}$ increases the time the solution will oscillate.

7.3 Stability analysis for $\alpha = 3$

A binary search has found $A_{critical} = 75.4999145847602406$ as the threshold of blackhole formation. In the previous chapter, Matlab found $16 < A_{critical} < 17$. This discrepency is because different widths were given for the initial gaussians.

By giving the NSP system $A_{critical}$ as an initial condition, $\Psi_{critical}$ has been found to oscillate as shown in Fig. 7.2. Our critical solutions are only as good as the accuracy of $A_{critical}$, as it can be seen in Fig. 7.2 the solution dispurces for larger t, our solutions will only be valid within the regions of oscillation.

In order to calculate the pertubation, the oscillations seen Fig. 7.2 must be removed, revealing the fundamental solutions which are stable in time; That is the static solutions calculated in chapter 4. A plot of the fundamental solutions $\Psi_{critical}(0,t)$ vs t would ideally produce a constant line, while a radial plot will produce the static solutions seen from chater 3 and 4.

The way we have decided to remove the oscillations, is to take a time average of our solution at $r = 0$, defined as

$$\overline{\Psi}(0,t) = \frac{1}{\delta t}\int_{t-\frac{\delta t}{2}}^{t+\frac{\delta t}{2}} \Psi(0,\tau)\, d\tau \tag{7.9}$$

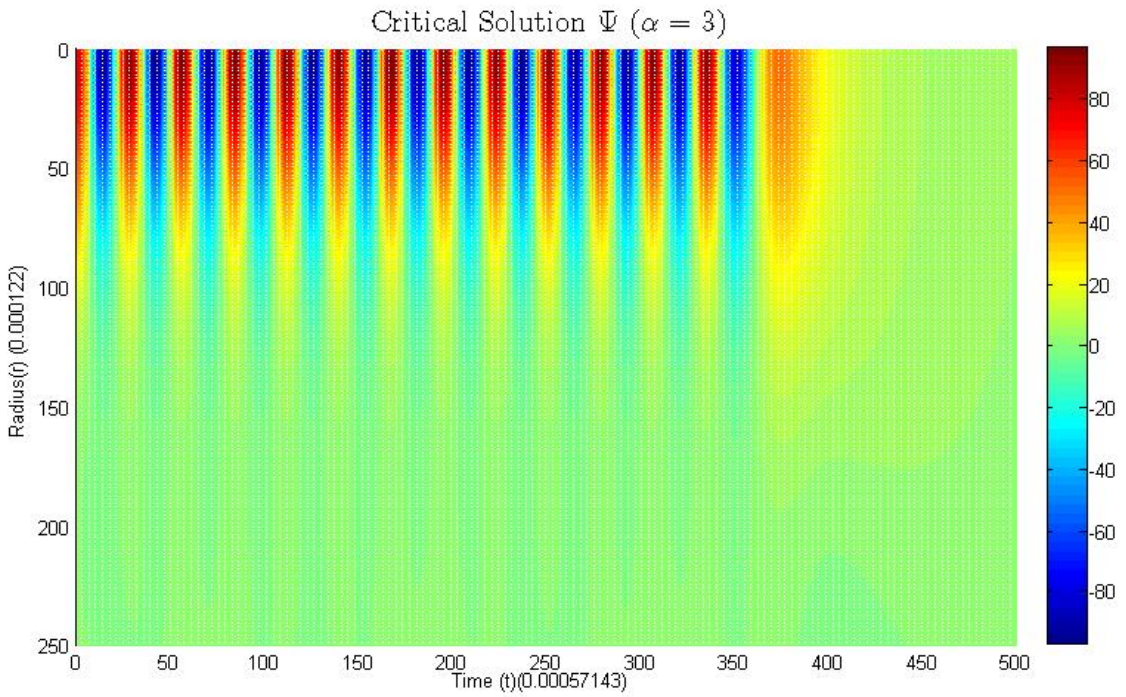

Figure 7.2: This plot shows the periodicity of our critical solution. The radial profile of Real(Ψ) can be seen to quickly decays.

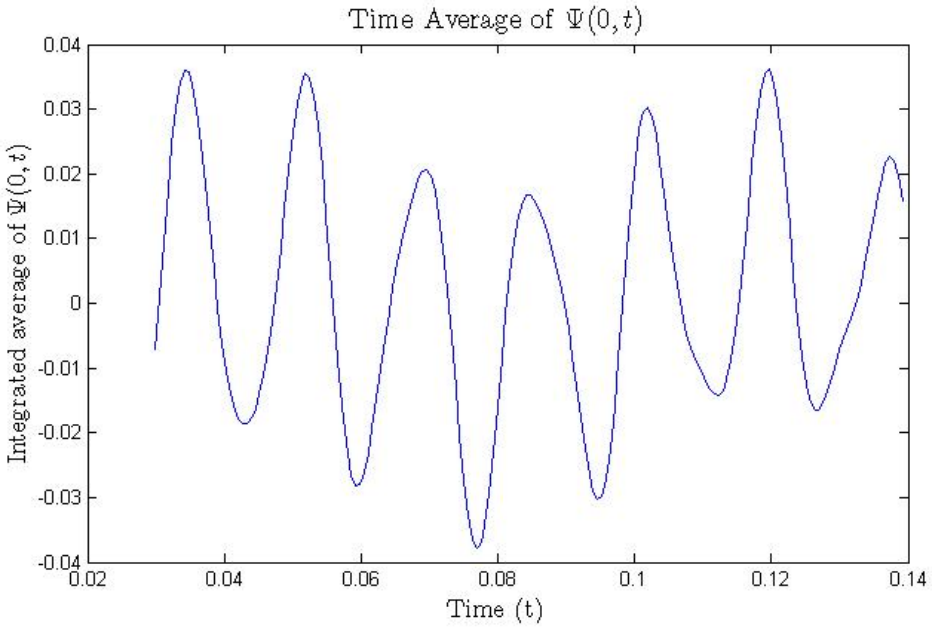

Figure 7.3: This plot shows the time average of the critical solution. While oscillations still exist, it can be seen that the solutions seems to have a minimum around 0.9. This is the point of closest approach between the critical solution and the static solution.

This integral has the property of averaging $\Phi(0,t)$, in theory eliminating the oscillations. To implement this numerically, δt will be given the value $n\omega$, where ω is the frequency of oscillations seen in Fig. 7.2 and n is an integer. For the following calculations, $\delta t = \omega = 0.0170898$. Equation (7.9) has been calculated using the mid point rule, yeilding

$$\overline{\Psi}(0,t^n) = \frac{1}{\delta t^n}\sum_{i=0}^{\delta t^n}\left(\Psi\left(0, i + t^n - \frac{\delta t^n}{2}\right) + \Psi\left(0, i+1+t^n - \frac{\delta t^n}{2}\right)\right)\frac{\Delta t}{2} \tag{7.10}$$

where δt^n denotes the discrete range of integration for each t^n. Δt has been denoted as the spacial step $(t_{i+1} - t_i)$. Equation (7.10) has been implemented over each discrete t^n value, creating an average over some region. The range of integration for $\overline{\Psi}(0,t)$ can be seen on Fig. 7.3.

Fig. 7.3 has been plotted showing $\overline{\Psi}(0,t)$, and will be used to obtain the time of closest approach between $\Psi_{critical}(r,t)$ and $\Psi_c(r)$, where $\Psi_c(r)$ is the static solution which occurs at time $t = t_c$. It can be seen in Fig. 7.3 that our averaging still has some oscillation, however, these oscillations have been reduced $\sim$1000 times from the origonal solution and have produced workable results. By definition, t_c occurs when $\frac{d\overline{\Psi}}{dt}(0,t) = 0$; t_c can be seen to lie between $t = 0.07$ and $t = 0.9$ by following the centre of the oscillations, and we will take $t_c = 0.8911$ for the following calculations.

With $\overline{\Psi}(r,t)$ and t_c calculated, we are in the position to define the pertubation as

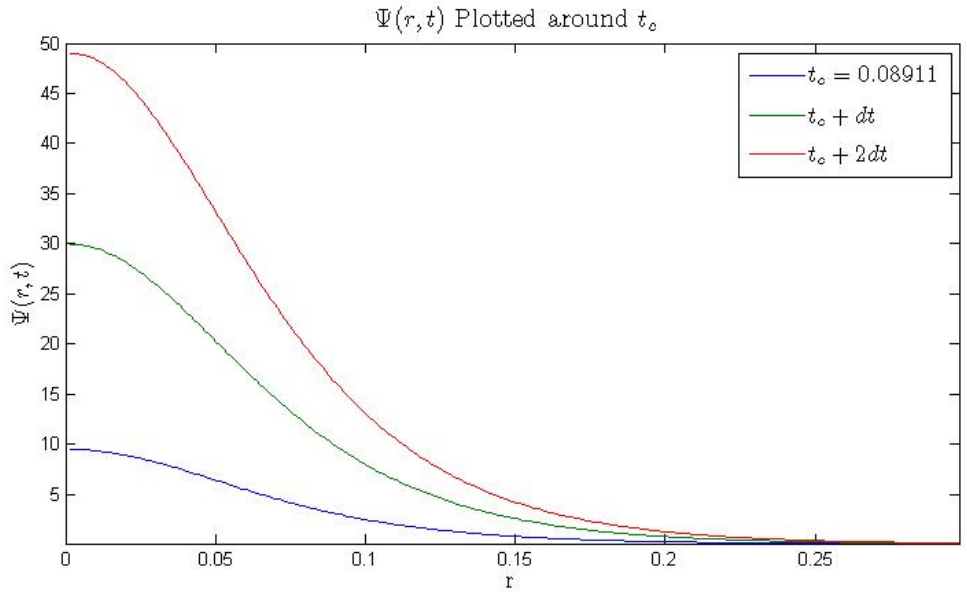

Figure 7.4: As $\Psi(r,t)$ approaches the static solution $\Psi(r,t_c)$ it can be seen that the static solution has a stable radial profile (no zero crossing).

$$\delta\Psi = e^{\lambda(t-t_c)}\delta\Psi_1(r) \tag{7.11}$$

Where $\delta\Psi_1(r)$ are static spacial profiles. It can be seen that λ will control whether $\delta\Psi$ is stable or instable; here we are looking for the same exponential behaviour as the static settings.

Fig. 7.4 shows the radial profile our our static solution $\Psi(r,t_c)$, $(\Psi(r,t_c) \equiv \Psi_c(r))$ before the oscillations have been removed, and some radial solutions around t_c. These radial profiles are all stable boson star solutions.

Fig. 7.5 shows the radial profile our our fundamental static solution $\overline{\Psi}(r,t_c)$, and some radial solutions around t_c. Here it can be seen that our radial profiles have gone from a stable boson star solutions to the 1-mode excited state. That is, the radial profiles for $\overline{\Psi}(r,t)$ cross the zero line once. This behaviour was expected from the static calculations, as we believed the static solutions switched from stable to 1-mode excited at $\alpha = \frac{8}{3}$ and now we have confirmed that, for $\alpha = 3$, we do indeed get 1-mode excited static solutions.

7.4 Results of Stability Analysis for $\alpha = 3$

Imputing all of the found data described in the last section has yielded $\lambda = 518 - 650i$. Plugging this value into equation (7.11), we can concude

$$\delta\Psi = e^{650i(t-t_c)}e^{518(t-t_c)}\delta\Psi_1(r) \tag{7.12}$$

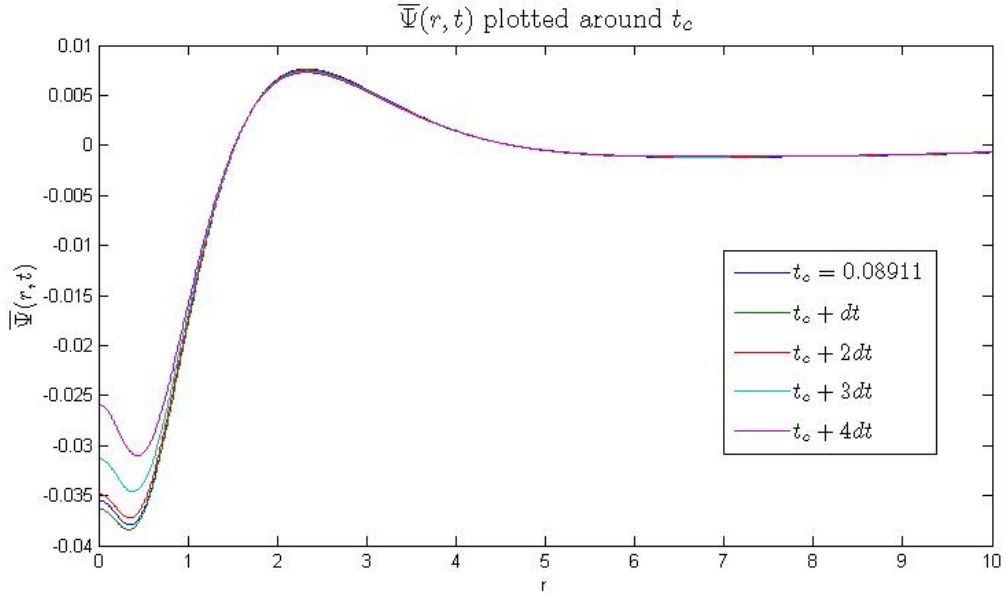

Figure 7.5: As $\overline{\Psi}(r,t)$ approaches the static solution $\overline{\Psi}(r,t_c)$ it can be seen the radial profiles have become 1-mode excited, revealing the fundamental solutions are unstable

When $(t - t_c) < 0$, $\overline{\Psi}(r,t)$ is approaching the static solution, and when $(t - t_c) > 0$, $\overline{\Psi}(r,t)$ is departing the static solution with some exponential behaviour (either growth or decay). $\delta\Psi_1(r)$ is some radial profile which is of no importance at this point.

To summarize the situation and results found here, we began by finding $\Psi_{critical}$ with $\alpha = 3$ in the NSP system. This corresponds to a 'star' having the perfect mass to remain stable (will not dispurse or collapse). From there, we are interested in introducing a small pertubation in our 'star', to see how the 'star' responds in our (NSP) system. It has been found through equation (7.12) that a small pertubation, denoted $\delta\Psi$, introduced at some time ($t = 0$), will exhibit exponential growth for all time $(t - t_c) > 0$; That is, our 'star' will become unstable.

Chapter 8

Conclusion

This project began with the goal of building a mathematical model that was capable of describing matter coupled to gravity using scalar fields. The purpose was to study the system in hopes of learning more about critical phenomenon.

We began by defining our model with a parameter α that allowed us to control the strength of gravity. Then by making the correct anzats to convert the system into a static setting, it was found that two distinctly different end behaviours occured when looking at mass as a function of central pressure. The boundary of these two behaviours was founds to be $\alpha = 8/3$, denoted α_c. Through smoothness of our static mass function, it was conjectured that $\alpha < \alpha_c$ produces stable solutions, while $\alpha > \alpha_c$ produces 1-mode unstable static solutions.

A static stability test was attempted by introducing a small pertubation in the fields. If exponential decay occured than the conclusion is stable solutions exist, and exponential growth would conclude 1-mode unstable solutions. Unfortunatly, neither behaviour was present, pushing us to use time dependent pertubation

Before looking at time dependent pertubation, it was vital to look at our system to confirm the static setting conclusions. setting $\alpha = 2$ displayed fields with initial growth followed by decay, alway dispursing at large time. $\alpha = 3$ showed dispursal for small initial amplitudes, and 'blow-up' for larger amplitudes. A binary search found our critical amplitude $A_{critical}$=75.4999145847602406, which produced the critical solution.

Time dependent stability analysis was done on our critical solution for $\alpha = 3$. First we had to remove the oscillations in the solution, in order to look at the fundamental solution. It was found that $\delta\Psi = e^{650i(t-t_c)}e^{518(t-t_c)}\delta\Psi_1(r)$ which exhibits exponential growth, showing $\alpha = 3$ is 1-mode unstable.

Combinding the static and time dependent results, we can confirm our conjecture that $\alpha < \alpha_c$ produces stable solutions, while $\alpha > \alpha_c$ corresponds to 1-mode unstable solutions.

Chapter 9

Future Work

The stability of $\alpha = \alpha_c$ was not tested purely due to time constraints, all of the theory and programs are done to do this test. It would be interesting to see if blow-up can occur in this region. Further, to show that there truely is a boundary at $\alpha = \alpha_c$; It may be of interest to show the behaviour of $\alpha = \alpha_c \pm \epsilon$ in time dependent settings, where ϵ is taken to be small.

Bibliography

[1] M.W.Choptuik, "Universality and scaling in the gravitational collapse of a scalar field". Phys. Rev. Lett. 70, 1993

[2] C.Gundlach, "Understanding critical collapse of a scalar field". Phys. Rev. Lett. Vol. 55 Num. 2 1997

[3] A.Inwood, "Critical Collapse of a Massive Scalar Field in Newtonian Gravity". Thesis, The University of British Columbia, 2009

[4] K.Lai, "A Numerical Study of Boson Stars". PhD. Thesis, The University of British Columbia, 2004

[5] Dae-Il Choi, "Numerical Studies of Nonlinear Schrödinger and Klein-Gordon Systems: Techniques and Applications". PhD. Thesis, The University of British Columbia, 1998

[6] M.W.Choptuik, Personal communication 2009

[7] Roger Penrose. Revistas del Nuovo Cimento, 1(252), 1969

[8] S. H. Hawley. Scalar Analogues of Compact Astrophysical Systems. PhD thesis, The University of Texas at Austin, 2000

[9] T.Harada, H. Maeda and B. Semelin, *Phys. Rev.*, **D67**, (084003), 2003

[10] Irene M. Moroz, Roger Penrose, and Paul Tod. Class. Quantum Grav., 15:2733 2742, 1998.

Appendix A

Static Solutions

The static solutions were all analyzed in Matlab. The build in program ODE45 was implemented to solve these couples ODE.

A.0.1 ODE

The first file defines the ODE. Equations (3.2) and (3.3) have been decomposed into first order ODE. Also, since the ODE become undefined at the origin, we were able to use L'Hpital's rule to obtain a bounded set of ODE when at the origin. These are described in the file below, with

- I = $\Phi(r)$
- J = $\frac{d}{dr}\Phi(r)$
- V = V(r)
- L = $\frac{d}{dr}V(r)$
- F = $\Phi_\epsilon(r)$ (perterbed field)
- K = $\frac{d}{dr}\Phi_\epsilon(r)$
- $V_D = V_\epsilon(r)$ (perterbed field)
- M = $\frac{d}{dr}V_\epsilon(r)$ (perterbed field)
- e = α (exponent to NSP system)
- w = ω (eigenfunction to $\Phi(r)$
- k = ω_ϵ (eigenfunction to $\Phi_\epsilon(r)$

Code

C is a comment line

clear all; format long Io = 25; Vo = 0; e = 3; C initial guess for w,k,rmax; program will fix w = 1; k = 1; rmax = 100; C ————START PROGRAM————- C columns of y = (I,J,V,L,F$_k$, $K, V_d, M, e, w, k)C - shootforw - fori = 1 : 190yin = [Io, 0, Vo, 0, Io, 0, Vo, 0, e, w, k]; rspan = [0, rmax]; [r, y] =$

$ode45('ODE', rspan, yin); I = y(:,1); for j = 1 : length(r); pow = 10^(-floor(i/10)); if I(j) > Io; w = w + pow; breakelseif I(end) - I(end-1) > 0; w = w + pow; breakelseif I(j) < 0; w = w - pow; breakelsew = wendendendCshiftVo, findshiftedwkk = find((y(:,2) < 0)); kkk = length(kk); rval = kkk-5; rmax = r(end); m = ((y(rval,3))); ws = w-m; CthisisshiftedwvalueVs = -abs(m)C-----replot-(correctIVwr1max)----------yin = [Io,0,Vs,0,Io,0,Vo,0,e,ws,k]; rspan = [0,rmax]; [r,y] = ode45('ODE', rspan, yin); I = y(:,1); V = y(:,3); [P,PP] = min(abs(I - 0)); r1max = r(PP); rspan = [0,r1max]; [r,y] = ode45('ODEP', rspan, yin); I = y(:,1); V = y(:,3); C------userr-----shootfork----alterVeo--------CfirstguessVeo = Vs+.3rmax = 150; for i = 1 : 190 yin = [Io,0,Vs,0,Io,0,Veo,0,e,ws,k]; rspan = [0,rmax]; [rr,y] = ode45('ODE', rspan, yin); F = y(:,5);$

for j = 1:length(rr); pow = $10^{(-floor(i/10))}$; $if F(j) > Io; k = k + pow; breakelseif F(j) < 0; k = k - pow; break$

A.0.2 Program

This program has α, $\psi(0)$, V(0), and $r_{\max}$ as free variables. Once these are defined, the program will first find ψ(r) and corresponding eigenvalue w to 16 decimal places, along with V(r). It will then find $\psi_\epsilon(r)$ along with corresponding eigenvalue w_ϵ, and $V_\epsilon(r)$.

Code

C is a comment line

clear all; format long Io = 25; Vo = 0; e = 3; C initial guess for w,k,rmax; program will fix w = 1; k = 1; rmax = 100; C ————START PROGRAM————- C columns of y = (I,J,V,L,F$_k$, K, V_d, M, e, w, k)C----------$shootforw$----------$fori = 1 : 190 yin = [Io,0,Vo,0,Io,0,Vo,0,e,w,k]; rspan = [0,rmax]; [r,y] = ode45('ODE', rspan, yin); I = y(:,1); for j = 1 : length(r); pow = 10^(-floor(i/10)); if I(j) > Io; w = w + pow; breakelseif I(end) - I(end-1) > 0; w = w + pow; breakelseif I(j) < 0; w = w - pow; breakelsew = wendendendCshiftVo, findshiftedwkk = find((y(:,2) < 0)); kkk = length(kk); rval = kkk-5; rmax = r(end); m = ((y(rval,3))); ws = w-m; CthisisshiftedwvalueVs = -abs(m)C-----replot-(correctIVwr1max)----------yin = [Io,0,Vs,0,Io,0,Vo,0,e,ws,k]; rspan = [0,rmax]; [r,y] = ode45('ODE', rspan, yin); I = y(:,1); V = y(:,3); [P,PP] = min(abs(I - 0)); r1max = r(PP); rspan = [0,r1max]; [r,y] = ode45('ODEP', rspan, yin); I = y(:,1); V = y(:,3); C------userr-----shootfork----alterVeo--------CfirstguessVeo = Vs+.3rmax = 150; for i = 1 : 190 yin = [Io,0,Vs,0,Io,0,Veo,0,e,ws,k]; rspan = [0,rmax]; [rr,y] = ode45('ODE', rspan, yin); F = y(:,5);$

for j = 1:length(rr); pow = $10^{(-floor(i/10))}$; $if F(j) > Io; k = k + pow; breakelseif F(j) < 0; k = k-pow; breakelsek = k; endkendendC--(correctIVwr1max)---replot--(getr2maxVeF)-$--------$yin = [Io,0,Vs,0,Io,0,Veo,0,e,ws,k]; rspan = [0,rmax]; [r,y] = ode45('ODE', rspan, yin); F =$

$y(:,5); Ve = y(:,7); k2 = find(abs(y(:,8) > 3)); r2max = r(k2(1) - 5);$
yin=[Io,0,Vs,0,Io,0,Veo,0,e,ws,k]; rspan=[0,r2max]; [r, y]=ode45('ODE', rspan, yin); I = y(:,1);
V = y(:,3); rspan=[0,r2max]; [rr, y]=ode45('ODE', rspan, yin); F = y(:,5); Ve = y(:,7); C ———
—-PLOT————— plot(r,I,rr,F,r,V,rr,Ve) legend('Φ','Φ_ϵ','V','V_ϵ')$title('Solutionswithperturbations')xlabe$

Appendix B

Time Dependent Solutions

B.1 Time Dependent Solutions using Matlab

The build in program PDEPE was implemented for the time dependent calculations. PDEPE is specifically designed to solve PDE of the form

$$c\left(x,t,u,\frac{\partial u}{\partial x}\right)\frac{\partial u}{\partial t}=x^{-m}$$

$\partial_{\overline{\partial x}}$

$\left(x^m f\left(x,t,u,\frac{\partial u}{\partial x}\right)\right)+s\left(x,t,u,\frac{\partial u}{\partial x}\right)$ (B.1)Since we are working with spherically symetric coordinates, m=2. NSP is a set of two PDE of the form set by equation (B.1). This program consisted of four seperated .m files which are described below.

B.1.1 Boundary Conditions

MATLAB function that defines boundary conditions for a system of two PDE in time and one space dimension. The boundary conditions are written in the form

$$p\left(x,t,u\right)+q\left(x,t\right)f\left(x,t,u,\frac{\partial u}{\partial x}\right)=0 \tag{B.2}$$

which yields the following matlab file for the boundary conditions:

```
function [pl,ql,pr,qr] = bc2(xl,ul,xr,ur,t)
pl = [0; 0];
ql = [1; 1];
pr = [ur(1); ur(2)];
qr = [1; 1];
```

B.1.2 Initial Conditions

The two fields ($\Phi(r)$ and $V(r)$) are given an initial shape. $\Phi(r)$ is chosen to be a positive gaussian and $V(r)$ is the negative gaussian, as those are the shapes we were getting with the static solutions.

function value = initial(x)
global A
value = [A*exp(-(x^2/0.05)); $-A * exp(-(x^2/0.05))$];

B.1.3 PDE Equations

The equations for the NSP system given in the form of equation (B.1) are:

function [c,b,s] = eqn(x,t,u,DuDx)
global eps;
c = [i; 0];
b = [-1/2 ; 1] .* DuDx;
s = [u(1)*u(2) ; -(abs(u(1)))$^e ps$];

B.1.4 Program for Time Dependent Calculations

clear all
format long
global eps A

eps = 2;
A = 30
N = 200
for i = 1:N
x(i)=2*(1-cos(i*pi/(2*N)));
end
TEND = 0.2
t = linspace(0,TEND,2000);
m = 2;
sol = pdepe(m,@eqn,@initial,@bc,x,t);
Φ(r,t) = sol(:,:,1);
V(r,t) = sol(:,:,2);

B.2 Independent Residual (convergence)

While a pre-programmed MATLAB code has been chosen, it is important to check the convergence of our PDE. To do so, I will begin by taking our Schrödinger equation and replace the V term

Figure B.1: Taking the difference between the independent residual of decreasing mesh points, we get $I(dr, dt) - I(\frac{dr}{2}, \frac{dt}{2}) = 37$, $I(\frac{dr}{2}, \frac{dt}{2}) - I(\frac{dr}{4}, \frac{dt}{4}) = 33$, $I(\frac{dr}{4}, \frac{dt}{4}) - I(\frac{dr}{8}, \frac{dt}{8}) = 19$ indicating convergence of our system.

with a constant called 'N'.

$$\frac{\partial \Psi\left(r,t\right)}{\partial t} = -\frac{1}{2}\Delta\Psi\left(r,t\right) + N\Psi\left(r,t\right) \tag{B.3}$$

Now we have an equation which depends only on $\Psi(r,t)$. The next step is to use the spherically symetric laplacian, and break our equation in discrete time and space steps.

$$\frac{1}{2}\frac{\Psi_j^{n+1} - \Psi_j^{n-1}}{\Delta t} = -\frac{1}{2}\frac{1}{r_j^2}\left(r_{j+\frac{1}{2}}^2\left(\frac{\partial\Psi}{\partial r}\right)_{j+\frac{1}{2}}^n - r_{j-\frac{1}{2}}^2\left(\frac{\partial\Psi}{\partial r}\right)_{j-\frac{1}{2}}^n\right) + N\Psi_j^n \tag{B.4}$$

where j is the spacial and n is the time step. You will notice that some of the spacial steps are takin in half integers, which do not exist. This was done to allow a central difference operator to be used on the radial derivitives.

$$\frac{1}{2}\frac{{\Psi_j}^{n+1} - {\Psi_j}^{n-1}}{\Delta t} = -\frac{1}{2}\frac{1}{{r_j}^2\Delta r^2}\left(r_{j+\frac{1}{2}}^2\left(\Psi_{j+1}^n - \Psi_j^n\right) - r_{j+\frac{1}{2}}^2\left(\Psi_j^n - \Psi_{j-1}^n\right)\right) + N\Psi_j^n \tag{B.5}$$

with $r_{j+\frac{1}{2}} \equiv \frac{1}{2}\left(r_{j+1} + r_j\right)$ and $r_{j-\frac{1}{2}} \equiv \frac{1}{2}\left(r_j - r_{j-1}\right)$

The independent Residual (I) is taken to be the difference between the two sides of the equation.

$$I = \frac{1}{2}\frac{{\Psi_j}^{n+1} - {\Psi_j}^{n-1}}{\Delta t} + \frac{{\Psi_j}^{n+1} - {\Psi_j}^{n-1}}{2\Delta t} + \frac{1}{2}\frac{1}{{r_j}^2\Delta r^2}\left(r_{j+\frac{1}{2}}^2\left(\Psi_{j+1}^n - \Psi_j^n\right) - r_{j+\frac{1}{2}}^2\left(\Psi_j^n - \Psi_{j-1}^n\right)\right) - N\Psi_j^n \tag{B.6}$$

And for convergence to occur, scaling the mesh to finer grid points should converge I to some function. Convergence brings us to a scaled function and not to zero due to the constant N that was introduced to eliminate the gravitational field dependency in the PDE. The above formula was coded in MATLAB with the mesh points taken to be successively smaller. Fig. B.1 showed a scaled function converging for successively smaller dr and dt, consistant with a converging solution; Thus we have convergence and can continue with the calculations.

B.3 Time Dependent Solutions using RNPL

To calculate the critical solutions ($\Psi_{critical}$) with $\alpha = 3$, I used Andrew Inwoods RNPL code. Convergence has been discussed in his thesis [3].